Published in final edited form as:
J Am Chem Soc. 2009 November 4; 131(43): 15711–15716. doi:10.1021/ja9046697.

Structural and Functional Studies of *A. oryzae* Cutinase: Enhanced Thermostability and Hydrolytic Activity of Synthetic Ester and Polyester Degradation

Zhiqiang Liu[1], **Yuying Gosser**[2], **Peter James Baker**[1], **Yaniv Ravee**[1], **Ziying Lu**[2], **Girum Alemu**[2], **Huiguang Li**[3], **Glenn L. Butterfoss**[4], **Xiang-Peng Kong**[3], **Richard Gross**[1], and **Jin Kim Montclare**[1,5,*]

[1]Department of Chemical and Biological Sciences, Polytechnic Institute of New York University, Brooklyn, NY 11201

[2]Pathways Bioinformatics & Biomolecular Center, The City College, CUNY, New York, NY 10031

[3]Department of Biochemistry, NYU School of Medicine, 550 First Avenue, New York, NY 10016

[4]Department of Biology and Computer Science, New York University, New York, NY 10003

[5]Department of Biochemistry, SUNY-Downstate Medical Center, Brooklyn, NY 11203

Abstract

Cutinases are responsible for hydrolysis of the protective cutin lipid polyester matrix in plants and thus have been exploited for hydrolysis of small molecule esters and polyesters. Here we explore the reactivity, stability, and structure of *Aspergillus oryzae* cutinase and compare it to the well-studied enzyme from *Fusarium solani*. Two critical differences are highlighted in the crystallographic analysis of the *A. oryzae* structure: (*i*) an additional disulfide bond and (*ii*) a topologically favored catalytic triad with a continuous and deep groove. These structural features of *A. oryzae* cutinase are proposed to result in improved hydrolytic activity and altered substrate specificity profile, enhanced thermostability and remarkable reactivity towards the degradation of the synthetic polyester, polycaprolactone. The results presented here provide insight into engineering new cutinase-inspired biocatalysts with tailor-made properties.

Keywords

A. oryzae; cutinase; hydrolysis; substrate specificity; thermostability; disulfide bond; polyester degradation

INTRODUCTION

With environmental concerns over waste build-up and limited petroleum resources, the demand has never been greater for enzymatic, or “green” approaches for efficient chemical synthesis and degradation reactions.[1–3] Several enzymes have been exploited to not only perform stereo- and regioselective chemical transformations on small molecules, but also to breakdown or modify synthetic polymers useful for applications in chemical, pharmaceutical and textile

*jmontcla@poly.edu.

Supporting Information Available. SDS PAGE, CD and DSC characterization and kinetics is available free of charge via the Internet at http://pubs.acs.org.

industries,[2, 4, 5] Serine hydrolases have been employed most extensively for these biotransformations.[1, 6–14]

Cutinases are α/β hydrolases commonly secreted by fungal phytopathogens that enable them to penetrate the protective surface cutin layer of plants.[15–19] Cutin is an insoluble, crosslinked, lipid-polyester matrix comprised of n-C_{17} and n-C_{18} hydroxy and epoxy fatty acids that serve as a barrier from dehydration and invasion. Cutinases hydrolyze and breakdown these complex polyesters into smaller hydroxyacids.[15, 19]

Due to the ability of cutinases to hydrolyze cutin, they have been exploited for reactions with small molecule esters and synthetic polyesters.[1] The utility of cutinase or any enzyme for chemical reactions is commonly limited by intolerance to high temperatures and the constraints of the substrate recognition pocket.[1] Thus, the identification of enzymes exhibiting enhanced thermostability and altered reactivity for various substrates would greatly expand the potential of cutinase for industrial and environmental applications.

A. oryzea is a filamentous fungus that has been employed in fermentation to produce traditional consumable products such as rice wine, soybean paste and soy sauce in the food industry for approximately 1000 years.[9] It has been used recently as an expression host for recombinant proteins[20] and to degrade poly-(butylene succinate) (PBS) as well as emulsified poly(butylenes succinate-co-adipate) (PBSA).[3] Because of the remarkable ability of *A. oryzae* cutinase to readily breakdown such synthetic plastics,[3] it represents an excellent target to perform detailed structure-activity analysis. Here we report the reactivity, stability and crystal structure of *A. oryzea* cutinase as well as perform a comparison to the well-characterized *F. solani* cutinase.

METHODS

Enzymes Expression

The cutinase gene was expressed in *Pichia pastoris*, and recombinant cutinase was produced by using the strong methanol-induced AOX1 promoter. The single colonies were picked and cultured in BMGY medium (g/L) composed of 5 g yeast extract, 10 g peptone, supplemented with 50 mL 1M KH_2PO_4 buffer pH 6.0, 1.7 g yeast nitrogen base, 5 g ammonium sulfate, 5 mL glycerol, 500 × l mL biotin 96 × 5.2 mL histidine. Precultures of *Pichia pastoris* harboring cutinase genes were incubated at 30 °C, 200 rpm, overnight. After centrifugation at 6,000 rpm for 10 min, cells were transferred into a parallel fermentor (DASGIP, Germany) containing 1 L basal salt medium composed of glycerol 40 mL/L, $CaSO_4$ 0.9 g/L, K_2SO_4 14.67 g/L, $MgSO_4$ $7H_2O$ 11.67 g/L, $(NH_4)_2SO_4$ 9 g/L, 12 mL/L hexametaphosphate, trace salts (cupric sulfate $5H_2O$ 6.0 g/L, sodium iodide 0.08 g /L, manganese sulfate H_2O 3.0 g/L, sodium molybdate $2H_2O$ 0.2 g/L, boric acid 0.02 g/L, cobalt chloride 0.5 g/L, zinc chloride 20.0 g/L, ferrous sulfate $7H_2O$ 65 g/L, biotin 0.2 g/L). The constant dissolved oxygen was set to 40%, glycerol (50%, v/v) feeding time was 6 h and the rate of methanol feeding was 5 mL/h. When the activity reached its maximum, the fermentation was stopped. After centrifugation, the supernatant was collected for further use.

Enzyme Purification

Fermentation broth was centrifuged at 8,000 rpm for 10 min at 4°C, and then supernatant was concentrated about 10 times using an ultrafiltration unit (Millipore TFE system) with a 10 kDa membrane. Cutinase were purified by FPLC using VISION™ Workstation (Applied Biosystems Co.) with a 16 mmD/100 mmL POROS® MC 20 μm column (Applied Biosystems Co.). The metal site in column was saturated by $NiCl_2$ solution according to operating instructions of column. Approximately, 50 mM NaH_2PO_4 buffer with 0.5 mM imidazole (pH 8.0) was used as a starting buffer and 50 mM NaH_2PO_4 buffer with 100 mM imidazole (pH

8.0) was used as an elution buffer at a flow rate of 30 mL/min. Samples filtered by a 0.45 μm filter were loaded onto the column. Approximately 2 column volumes (CV) of starting buffer was run to wash out any proteins which were bound non-specifically to the column, and then 3 CV elution buffer with imidazole was run with concentration linear gradient from 0 to 100 mM. The peak fraction in the gradient step was collected. The collected samples were desalted by an ultrafiltration unit with a 10 kDa membrane and then freeze-dried. SDS PAGE analysis of the purified proteins were performed (Supporting Information).

Kinetic analysis for pNP ester substrates

The pNP esters (pNPA, pNPB, pNPV and pNPH) with concentration ranging from 60 μM to 0.9375 μM were used for the kinetic study.[21, 22] Assays were performed using a final concentration of 1.1 μM of *A. oryzae* and *F. solani* cutinases in 14.5 mM Tris-HCl buffer pH 7.5, 0.75% glycerol. Since pNPA and pNPH were dissolved in DMSO, pNPB in methanol and pNPV in TritonX, there was approximately 25% of DMSO, methanol or 0.5% Triton X in the final mixtures.[23] Reactions were initiated by the addition of enzyme and reaction progress was monitored spectrophotometrically (Molecular Devices Spectramax M2) at 405 nm. Softmax Pro v5 software was used to analyze data. Enzyme-catalyzed initial rates were corrected by subtracting background hydrolysis rate. All reactions were performed in triplicate. The K_m and k_{cat} values were determined by a double-reciprocal Lineweaver-Burk plot (1/v vs. 1/[pNPA/ pNPB/ pNPV/ pNPH]) (Supporting Information).

Thermoactivity

The thermoactivity or residual activity of cutinases were investigated by incubating enzymes at temperatures ranging from 25°C to 60°C at a final concentration of 1.1 μM in 14.5 mM Tris-HCl buffer pH 7.5, 0.75% glycerol. The incubation took place in an Eppendorf Thermomixer at the specified temperature with a constant mixing of 350 rpm for an hour. The samples were incubated on ice for 5 minutes followed by incubation at room temperature for 15 minutes. Reactions were initiated by addition of 30 μM pNPB and monitored at 405 nm for 1 minute and performed in triplicate. The data obtained was presented as activity without normalization.

Circular dichroism (CD) measurements

CD spectra were recorded on a JASCO J-815 Spectropolarimeter using Spectra Manager 228 software. Temperature was controlled using a Fisher Isotemp Model 3016S water bath. A protein concentration of 29 μM in 10 mM sodium phosphate buffer, pH 8.0 was used for both cutinases. Data were collected at 1-nm intervals from 190 nm to 250 nm for wavelength scans and 0.3°C/min from 4°C to 85°C for temperature scans in duplicate (Supporting Information). Small signaling arising from buffer was subtracted.

Thermodynamic parameters by differential scanning calorimetry (DSC)

Calorimetric measurements of melting temperatures (T_m) were carried out on a NanoDSC differential scanning calorimeter (TA Instruments) with a sample cell volume of 0.3 mL. Unfolding data of both cutinases were obtained by heating the samples, at a concentration 5 mg/mL, from 4 to 80°C at a rate of 1°C/min in duplicate (Supporting Information). The protein samples were present in water. Water was used in the reference cell to obtain the molar heat capacity by comparison. The observed thermograms were baseline corrected and normalized data were analyzed using NanoAnalyze software.

Degradation of polymer thin films

Thin film of poly(ε-caprolactone) (PCL) were cut into (1.0 × 1.0 cm) with an approximate thickness of 250 μm (30–35 mg) and placed in 20 mL scintillation screw cap vials containing 2.5 mL of 80 mM Tris-HCl buffer pH 8.0 with a final concentration of 8.8 μM enzyme. The

control vials contained a film with buffer solution. All measurements were performed in triplicate and incubated for 6 hrs at 40°C in an incubator shaker at 200 rpm and weighed after drying.

Crystallization

The protein was crystallized by mixing equal volumes of protein solution (15 mg/mL, in 100 mM Tris buffer pH 8.5) with mother liquor (30% PEG2KMME, 100 mM potassium thiocyanate) at 296 K. The screening was conducted with 96 crystallization conditions at 296K using the hanging drop vapor diffusion technique. Crystals appeared within 10–15 days.

Structure Determination

X-ray diffraction data of the crystal was collected at beamline X4A (λ =0.96785 Å) of synchrotron light source in Brookhaven National Laboratory. Prior to data collection, the crystal was soaked for 5 minutes in a mixture of the mother liquid (30% PEG2000MME and 100 mM potassium thiocyanate) and 15% glycerol for cryoprotection. A data set of 1.75 Å resolution was collected from a single crystal at 100K with 98.5% completeness. This data set was processed using HKL2000 software.[24] The crystal belongs to the trigonal space group $P3_221$ with one subunit in the asymmetric unit. The unit cell parameters a=45.299, b=45.299, c=157.111 and α90.00, β90.00, χ120.00. The structure was solved by molecular replacement using the Molrep program in the CCP4 suite.[25] The structure of the native *F. solani* cutinase (PDB accession number 1CEX) was used as the search model. The initial model was built using O program. The structure was refined with CNS.[26] The iterative model building and refinement was carried out to a final R-work factor of 19.4% and a final free-R factor of 19.9%. The stereochemistry of the final structure was verified using the Procheck_NT and Sfcheck programs in the CCP4 suite.[25] Procheck validation of local geometry revealed that 91.5% residues are located in the most favored regions of the Ramachandran plot, 7.2% are in the additional allowed regions, and 1.3% are in the generously allowed region. The electron densities of the first 10 N-terminal residues (17–25) were not observed. Structural analysis was performed using UCSF Chimera software http://www.cgl.ucsf.edu/chimera.[27] Electrostatic surface rendering was performed using ICN and the groove by the active site was generated by the PocketFinder function.[28] For all above analysis 1CEX pdb file was used for *F. solani* cutinase.

Modeling

1CEX and the crystal structure presented here were modeled with the butyrate, valerate, and hexanoate esters of the active site serine. Hydrogens were added and starting structures of the serine esters were generated by sampling all combinations of −60, 60, and 180 degrees for each chi angle (with the exception of the ester C-O torsion, which was sampled at −180 and 180). This generated 162, 486 and 1458 conformations for the butyrate, valerate and hexanoate esters, respectively. The modified serine residues were then subject to 11 times 20 steps of conjugate gradient energy minimization using the CHARMM22 potential[29] while keeping all other protein atoms fixed. Modeling was done using the SIGMA package.[30]

RESULTS

Altered Specificity of *A. oryzae* Cutinase for pNP Esters

Initially, the *A. oryzea* and *F. solani* cutinases have been assessed for hydrolytic activity on a set of model *p*-nitrophenylester substrates: *p*-nitrophenylacetate (pNPA), *p*-nitrophenylbutyrate (pNPB), *p*-nitrophenylvalerate (pNPV), and *p*-nitrophenylhexanoate (pNPH) (Scheme 1a).[3,10] The influence of chain length on cutinase activity is studied via Michaelis-Menten kinetics. The *A. oryzea* cutinase demonstrates a preference for pNPV

resulting in a K_m of 0.04 ± 0.01 μM, followed by pNPB and pNPH with a K_m of 0.21 ± 0.04 and 0.29 ± 0.09 μM, respectively. The short pNPA chain yields a > 120 fold higher K_m of 4.96 ± 0.11 μM (Table 1). The highest catalytic efficiency is observed for pNPB and pNPV with a k_{cat}/K_m of 3.49 ± 0.51 and 3.32 ± 0.74 $\mu M^{-1}min^{-1}$ (Table 1). This is followed by pNPH and PNPA with a k_{cat}/K_m of 1.34 ± 0.48 and 0.07± 0.01 $\mu M^{-1}min^{-1}$, respectively. This is in stark contrast to *F. solani* cutinase, where an overall preference for short chain substrate pNPA was highest. Although recognition for all three substrates was relatively similar with K_m's ranging from 0.67 ± 0.23 to 1.50 ± 0.19 μM, the catalytic efficiencies reveal a strong preference for pNPA with a k_{cat}/K_m of 2.53 ± 1.11 $\mu M^{-1}min^{-1}$ followed by pNPV, pNPB and pNPH, respectively (Table 1). For pNPV, pNPB and pNPH, a 6, 10 and 20 fold decrease in k_{cat}/K_m is observed relative to pNPA.

Higher Thermostability of *A. oryzae* Cutinase

To investigate the ability of the two enzymes to function at higher temperatures, we examine the residual activities for pNPB hydrolysis for a range of temperatures. Selection of pNPB is based on the demonstration of reasonable reactivity by both cutinases. The *A. oryzea* cutinase exhibits a higher activity for pNPB relative to that of *F. solani* at room temperature corresponding to previous kinetic measurements. The level of activity is maintained even up to 40°C in the case of *A. oryzea* cutinase (Figure 1a). By contrast, *F. solani* enzyme reveals a 40% drop at 30°C and demonstrates a continuous decline in activity as a function of increasing temperature. Surprisingly, under all temperatures investigated, *A. oryzea* cutinase displays higher overall residual activity when compared to that of *F. solani*, suggesting an improved tolerance to heat. This is corroborated by thermostability measurements by circular dichroism (CD) in which *A. oryzea* cutinase exhibits a higher melting temperature (T_m) of 59°C, while the T_m of *F. solani* is 56°C (Table 1). This increase in T_m is manifested by a 60.4 kJ/mol increase in enthalpy by *A. oryzea* cutinase as measured by differential scanning calorimetry (DSC) (Table 1).

Higher Reactivity of *A. oryzae* Cutinase for Synthetic Polyester

Since the natural function of cutinase is to degrade the complex biopolyester of cutin,[15] we assess the ability of both *A. oryzae* and *F. solani* enzymes to react on the surrogate, well-defined polyester, poly ε-(caprolactone) (PCL) (Scheme 1b). PCL is known to be degraded by various microorganisms including fungi.[31, 32] Murphy and coworkers demonstrated that *F. solani* strains bearing cutinase were able to degrade PCL and use it as a carbon source--as well as induce the production of cutinase,[33] suggesting that the cutinase should be active for PCL hydrolysis *in vitro*. PCL films with dimensions of 1 cm_2 and 250 μm thickness were incubated at 40°C in the presence of either *A. oryzea* or *F. solani* cutinase in 100 mM Tris at pH 8.0. Remarkably, nearly complete degradation of 87% PCL is achieved within 6 hours in the presence of *A. oryzea* enzyme. Degradation of PCL films by *F. solani* cutinase proceeds slower reaching 30% degradation by 6 hours (Figure 1b). This data supports the results on the aforementioned substrate specificity in which the *A. oryzea* cutinase prefers longer chain esters such as pNPB and pNPH since PCL represents a longer chain polyester. Furthermore, this supports the thermoactivity data in which a dramatic loss in activity is observed for the *F. solani* enzyme at 40°C while that of *A. oryzae* maintains a high level activity.

Crystal Structure of *A. oryzae* Cutinase and Comparison to that of *F. solani*

To understand the observed reactivity and stability differences, the *A. oryzea* cutinase structure is determined by molecular replacement method and refined to 1.75 Å resolution (Supporting Information). The crystal structure reveals a monomeric protein with an α/ β fold hallmarked by a central β-sheet of 5 parallel strands surrounded by 10 α-helices. As a member of the α/β hydrolases, this enzyme possesses an active site comprised of the catalytic triad residues Ser

126, Asp 181 and His 194 (Figure 2a). The catalytic site is surrounded by the two hydrophobic surfaces comprised of residues 87–93 within helix 3, and residues 186–194 that represents the loop between helices 9 and 10 as well as the first 3 residues of the latter. *A. oryzea* cutinase bears an oxyanion hole comprised of Ser 48 and Gln 127 backbone amides that are critical in polarizing the ester bond of the substrate and stabilizing the transition state of the formed substrate oxyanion (Figure 2a).[12]

Upon overlay, the *A. oryzea* and *F. solani* structures have a similar fold with an overall rms deviation of 1.02 Å, main chain deviation of 0.87 Å and Cα deviation of 0.84 Å (Figure 3a). However, the *A. oryzae* enzyme bears several structural features that differ significantly from that of *F. solani*. Comparison of the two sequences reveal that the *A. oryzea* cutinase is shorter than that of *F. solani* as exhibited by smaller loops in the N- and C-terminal regions as well as a missing β-strand in the *A. oryzae* structure (Figure 2a, Figure 3a). Although the *F. solani* cutinase possesses 6 β-strands and 10 α-helices, the *A. oryzae* structure bears the 5 β-strands and the same number of α-helices. The N-terminal region (residues Thr 26 to Asp 30), the loops in between helix 1 and strand 1 (residues Gly 35 to Pro 49), as well as helix 2 and strand 2 (residues Ser 71 to Asp 73), helix 10 (residues Ser 199 to Asp 203), and C-terminal residues beyond helix 10 based on the *A. oryzae* structure deviate significantly in the overlay as highlighted in Figure 3a.

Distinct Disulfide Bond

The *A. oryzae* structure contains a unique disulfide bond between Cys 63-Cys 76 that ties helix 2 to strand 2 of the central β-sheet (Figure 2a). This disulfide bond has not been previously reported for any cutinase or hydrolase structures.[7, 12–17] The other two disulfide bonds, Cys 37-Cys 115 connecting the loop between helix 1 and strand 1 with the loop between helix 4 and strand 3, and Cys 177-Cys 184 linking the loop following strand 5 to helix 9 are well-conserved in previously published cutinase structures, including that from *F. solani*.[14] Sequence analysis suggests that this disulfide bond is unique for the cutinases from the *Aspergillus* family (sharing sequence identity of 50–77% with *A. oryzae*) and a few other filamentous fungi, such as *Neosartorya fischeri* (53% sequence iden*tity)* and *Emericella nidulans* 52% sequence identity) (Figure 2a). The cutinases from *F. solani* and *Glomerella cingulata* represent another group of filamentous fungi which do not have this special disulfide bond although they share about 50% sequence identity with the *A. oryzae* enzyme.

Continuous groove by the active site

Although the catalytic triad is sequentially conserved in the both cutinases, they are topologically positioned differently. In the *A. oryzea* structure, His 194 Nδ1 to Asp 181 Oδ2 is 2.71 Å, and the Ser 126 Oγ to His 194 Nε2 is 2.63 Å (Figure 3b)--which are within hydrogen bond distance. The corresponding distances in the *F. solani* cutinase are 2.84 Å for Asp 175 Oδ2 His 188 Nδ1, and 2.98 Å from Ser 120 Oγ to His 188 Nε2, which is slightly larger than the hydrogen bond distance presented in the *A. oryzae* structure.[16] This average distance of 2.98 Å was calculated based on the presence of two possible positions of the Ser 120 Oγ in the native *F. solani* crystal structure: where the A form possesses a 73% occupancy and the B form a 27% occupancy (Figure 3b). Moreover, the *A. oryzae* cutinase bears a longer and deeper groove by the active site relative to that of *F. solani* as demonstrated in Figure 3c. While the *A. oryzae* structure reveals a continuous groove that spans across the active site, the *F. solani* structure shows a narrow, shallower groove that abruptly stops. Models of both cutinases with the esters of the active site demonstrate the presence of two gatekeeper residues (Leu 87 and Val 190) in *A. oryzae* and (Leu 81 and Val 184) in *F. solani* that play a role in substrate recognition (Figure 4), The two residues in *A. oryzae* residues are 9.78 Å (Cβ to Cβ) apart while the corresponding residues of the *F. solani*. cutinase are separated by 8.74 Å. This results in the alkyl chain populations in *A. oryzae* laying across the wider groove region surrounding

the active site, while for the *F. solani* model, there is a preponderance of alkyl chain structures which are oriented down the narrow tail of the groove.

DISCUSSION

The molecular detail provided by the crystal structure elucidates the observed discrepancy in the activity and specificity by the two cutinases. The preference for the *A. oryzea* enzyme to hydrolyze longer chain substrates can be explained by the deep continuous groove extending across the active site, while that of *F. solani* favors short chain substrates due to the shallow and interrupted groove. This is further confirmed by our models demonstrating that the gatekeeper residues that line the groove within the *A. oryzae* are farther apart than the equivalent residues within the *F. solani* structure (Figure 4). In the *A. oryzae* structure, modeled with the hexanoate ester (Figure 4a), this additional space allows the carbon chains greater conformational freedom and easier access to a large region of the groove surrounding the active site. However, in the *F. solani* structure (Figure 4b), the close distance between the two gatekeeper residues creates a barrier, constraining the alkyl chains to a narrower region of the groove pointing away from the active site. The presence of a wider, continuous groove by the opening of the active site in *A. oryzae* cutinase can also explain its ability to rapidly hydrolyze PCL relative to that of *F. solani* (Figure 3c, 4a).

Enhanced thermotolerance is observed for *A. oryzae* cutinase by thermoactivity and thermodynamic stability experiments in comparison to that of *F. solani*. This improved stability can be attributed to the presence of an additional disulfide bond as observed in the *A. oryzea* structure (Figure 2b). Specifically, the disulfide bond between Cys 63-Cys 76 links a peripheral helix to the central β-sheet, providing extra stability. In general, covalent bonds stabilize proteins; specifically disulfide bonds connecting disparate and adjacent regions of a protein improves its thermostability.[34–36]

Understanding how the cutinase structure plays an important role in function and stability not only provides insight into the reactivity of *A. oryzae* enzyme, but also offers useful guidelines for the design of proteins in general. Much of the research on cutinases has thus far focused on employing that of *F. solani*. This is largely attributable to the existence of a crystal structure and extensive biochemical studies.[16, 18, 37–40] Recently, the structure of *Glomerella cingulata* cutinase has been determined, which suggests that the catalytic triad undergoes a significant conformational rearrangement during the catalytic cycle[41]--providing insight into its reactivity. Although a large number of *other* cutinases have been functionally investigated, [18, 37–40, 42–45] none have been structurally characterized and linked to their reactivities.

Cutinases have demonstrated unique properties that can be exploited for degradation of various synthetic polymers that may in the near future find use in plastic recycling.[46] Critical features highlighted in this work include: (*i*) engineering a continuous groove across the active site and (*ii*) including appropriate disulfide bonds as structural features that can be used in the redesign of other cutinases and related enzymes. From our studies, we have obtained useful guidelines for the re-design of proteins for environmentally compatible biocatalytic reactions on small molecules and polymer substrates useful for industry and academia.[1–3] Further detailed characterization to elucidate structural and functional information are underway.

Supplementary Material

Refer to Web version on PubMed Central for supplementary material.

Acknowledgments

This work was supported in part by NYU-Poly Seed Fund (XPK, YG, RG and JKM), AFOSR DURIP (FA-9550-08-1-0266) (JKM), IUCRC (RG), NSF GK-12 Fellows grant 0741714 (PJB), NIH grant GM70841 (HL and XPK) and the HHMI Science education project at CCNY (YG, ZL and GA). We thank Jeremy Minshull and Jonathan Ness from DNA 2.0 for their assistance with DNA and protein expression and purification optimization.

REFERENCES

1. Carvalho CML, Aires-Barros MR, Cabral JMS. Biotech. Bioeng 1999;66:17–34.
2. Guebitz GM, Cavaco-Paulo A. Trends Biotech 2008;26:32–38.
3. Maeda H, Yamagata Y, Abe K, Hasegawa F, Machida M, Ishioka R, Gomi K, Nakajima T. Appl Microbiol. Biotech 2005;67:778–788.
4. Costa L, Brissos V, Lemos F, Ribeiro FR, Cabral JMS. Bioproc. Biosys. Eng 2008;31:323–327.
5. Liu YB, Wu GF, Gu LH. AATCC Rev 2008;8:44–48.
6. Masaki K, Kamini NR, Ikeda H, Iefuji H. Appl. Environ. Microbiol 2005;71:7548–7550. [PubMed: 16269800]
7. Vidinha P, Harper N, Micaelo NM, Lourengo NMT, da Silva M, Cabral JMS, Afonso CAM, Soares CM, Barreiros S. Biotech. Bioeng 2004;85:442–449.
8. Borreguero I, Carvalho CML, Cabral JMS, Sinisterra JV, Alcantara AR. J. Mol. Cat. B-Enz 2001;11:613–622.
9. Bogel-Lukasik R, Lourenco NMT, Vidinha P, da Silva M, Afonso CAM, da Ponte MN, Barreiros S. Green Chem 2008;10:243–248.
10. Chen B, Hu J, Miller EM, Xie WC, Cai MM, Gross RA. Biomacromol 2008;9:463–471.
11. Kulshrestha AS, Gao W, Fu HY, Gross RA. Biomacromol 2007;8:1794–1801.
12. Chen B, Miller EM, Miller L, Maikner JJ, Gross RA. Langmuir 2007;23:1381–1387. [PubMed: 17241062]
13. Azim H, Dekhterman A, Jiang ZZ, Gross RA. Biomacromol 2006;7:3093–3097.
14. Hu J, Gao W, Kulshrestha A, Gross RA. Macromol 2006;39:6789–6792.
15. Purdy RE, Kolattukudy PE. Biochemistry 1975;14:2824–2831. [PubMed: 1156575]
16. Longhi S, Czjzek M, Lamzin V, Nicolas A, Cambillau C. J. Mol. Biol 1997;268:779–799. [PubMed: 9175860]
17. Sweigard JA, Chumley FG, Valent B. Mol. General Gen 1992;232:174–182.
18. Martinez C, Degeus P, Lauwereys M, Matthyssens G, Cambillau C. Nature 1992;356:615–618. [PubMed: 1560844]
19. Purdy RE, Kolattukudy PE. Biochemistry 1975;14:2832–2840. [PubMed: 239740]
20. Christensen T, Woeldike H, Boel E, Mortensen SB, Hjortshoejk K, Thim L, Hansen MT. Biotech 1988;6:1419–1422.
21. Pedersen S, Nesgaard L, Baptista RP, Melo EP, Kristensen SR, Otzen DE. Biopolymers 2006;83:619–629. [PubMed: 16964599]
22. Goncalves AM, Serro AP, Aires-Barros MR, Cabral JMS. Biochim. Biophy. Acta-Protein Struct. Mol. Enz 2000;1480:92–106.
23. Camacho RM, Mateo JC, González-Reynoso O, Prado LA, Córdova J. J. Indust. Microbiol. Biotech 2009;36:901–909.
24. Otwinowski Z, Minor W. Methods Enzym 1997;276:307–326.
25. Bailey S. Acta Cryst. Sect. D-Biol. Cryst 1994;50:760–763.
26. Brunger AT, Adams PD, Clore GM, DeLano WL, Gros P, Grosse-Kunstleve RW, Jiang JS, Kuszewski J, Nilges M, Pannu NS, Read RJ, Rice LM, Simonson T, Warren GL. Acta Cryst. Sect. D-Biol. Cryst 1998;54:905–921.
27. Pettersen EF, Goddard TD, Huang CC, Couch GS, Greenblatt DM, Meng EC, Ferrin TE. J. Comp. Chem 2004;25:1605–1612. [PubMed: 15264254]
28. Abagyan R, Totrov M, Kuznetsov D. J. Comp. Chem 2004;15:488–506.

29. MacKerell AD, Bashford D, Bellott M, Dunbrack RL, Evanseck JD, Field MJ, Fischer S, Gao J, Guo H, Ha S, Joseph-McCarthy D, Kuchnir L, Kuczera K, Lau FTK, Mattos C, Michnick S, Ngo T, Nguyen DT, Prodhom B, Reiher WE, Roux B, Schlenkrich M, Smith JC, Stote R, Straub J, Watanabe M, Wiorkiewicz-Kuczera J, Yin D, Karplus M. J. Phys. Chem. B 1998;102:3586–3616.
30. Mann, G.; Yun, RH.; Nyland, L.; Prins, J.; Board, J.; Hermans, J. In: Schlick, T.; Gan, HH., editors. Computational methods for macromolecules: Challenges and applications--Proceedings of the 3rd International Workshop on Algorithms for Macromolecular Modeling; Brelin. Springer Verlag; 2002. p. 129-145.
31. Benedict CV, Cook WJ, Jarrett P, Cameron JA, Huang SJ, Bell JP. J. Appl. Poly. Sci 1983;28:327–334.
32. Nishida H, Tokiwa Y. J. Environ. Polym. Degrad 1993;1:227–233.
33. Murphy CA, Cameron JA, Huang SJ, Vinopal RT. Appl. Env. Microbiol 1996;62:456–460. [PubMed: 8593048]
34. Pace CN. J. Mol. Biol 1992;226:29–35. [PubMed: 1619660]
35. Green SM, Meeker AK, Shortle D. Biochemistry 1992;31:5717–5728. [PubMed: 1610820]
36. Doig AJ, Williams DH. J. Mol. Biol 1991;217:389–398. [PubMed: 1992169]
37. Abergel C, Martinez C, Fontecillacamps J, Cambillau C, Degeus P, Lauwereys M. J. Mol. Biol 1990;215:215–216. [PubMed: 2213880]
38. Longhi S, Mannesse M, Verheij HM, DeHaas GH, Egmond M, KnoopsMouthuy E, Cambillau C. Protein Sci 1997;6:275–286. [PubMed: 9041628]
39. Longhi S, Nicolas A, Creveld L, Egmond M, Verrips CT, deVlieg J, Martinez C, Cambillau C. Proteins-Struct. Funct. Gen 1996;26:442–458.
40. Ettinger WF, Thukral SK, Kolattukudy PE. Biochemistry 1987;26:7883–7892.
41. Nyon MP, Rice DW, Berrisford JM, Hounslow AM, Moir AJG, Huang HZ, Nathan S, Mahadi NM, Abu Bakar FD, Craven CJ. J. Mol. Biol 2009;385:226–235. [PubMed: 18983850]
42. Nielsen AD, Arleth L, Westh P. Biochim. Biophys. Acta 2005;1752:124–132. [PubMed: 16162423]
43. Figueroa Y, Hinks D, Montero G. Biotech. Prog 2006;22:1209–1214.
44. Genencor Cutinase for use in detergent composition produced by culturing Pseudomonas putida. 1988.
45. Yoon MY, Kellis J, Poulose AJ. AATCC Rev 2002;2:33–36.
46. Seo HS, Um HJ, Min J, Rhee SK, Cho TJ, Kim YH, Lee J. Fems Yeast Res 2007;7:1035–1045. [PubMed: 17506831]

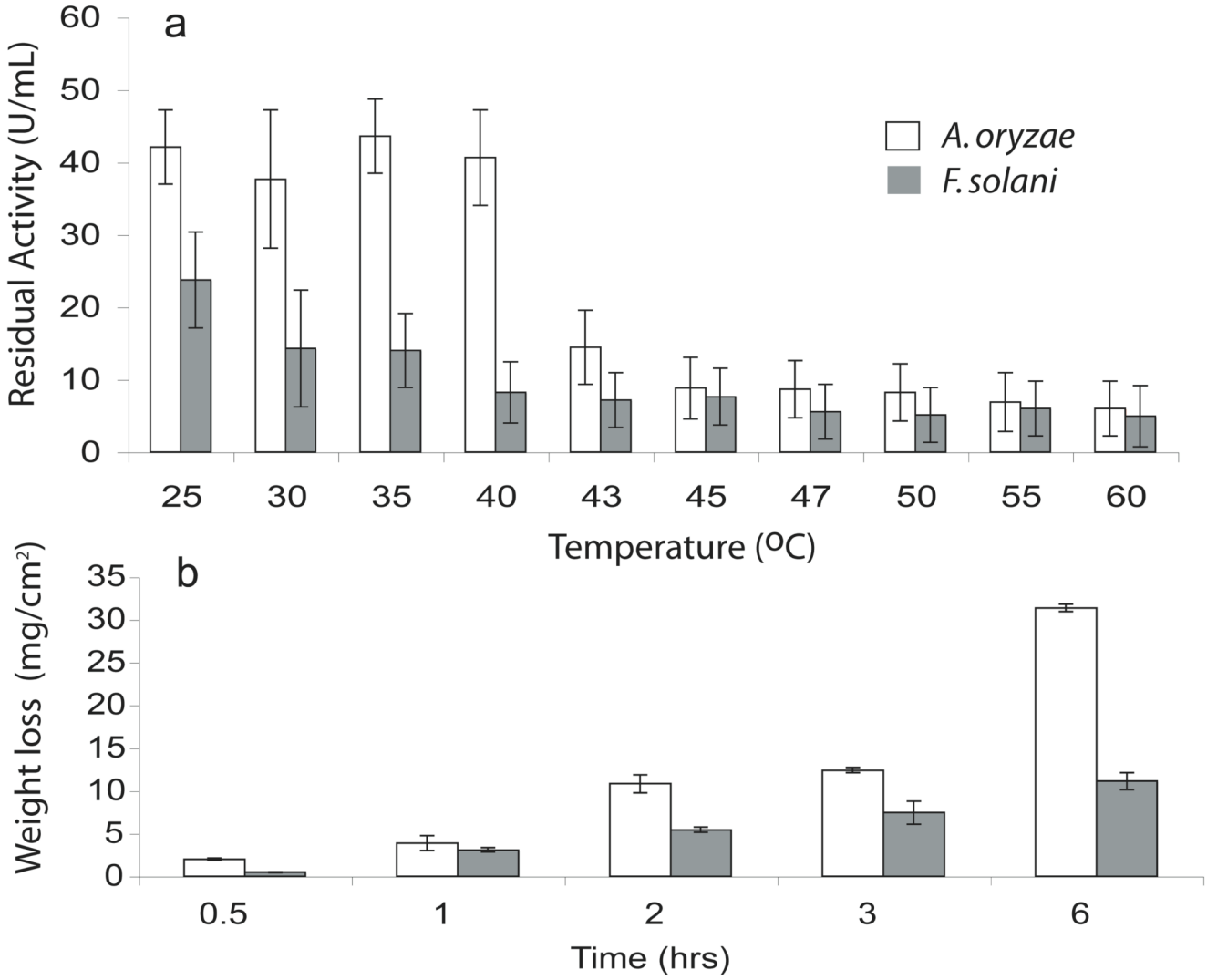

Figure 1.
(a) Thermoactivity profile as measured in terms of residual activity for pNPB upon incubation at increasing temperatures. (b) Weight loss measurements of defined PCL films.

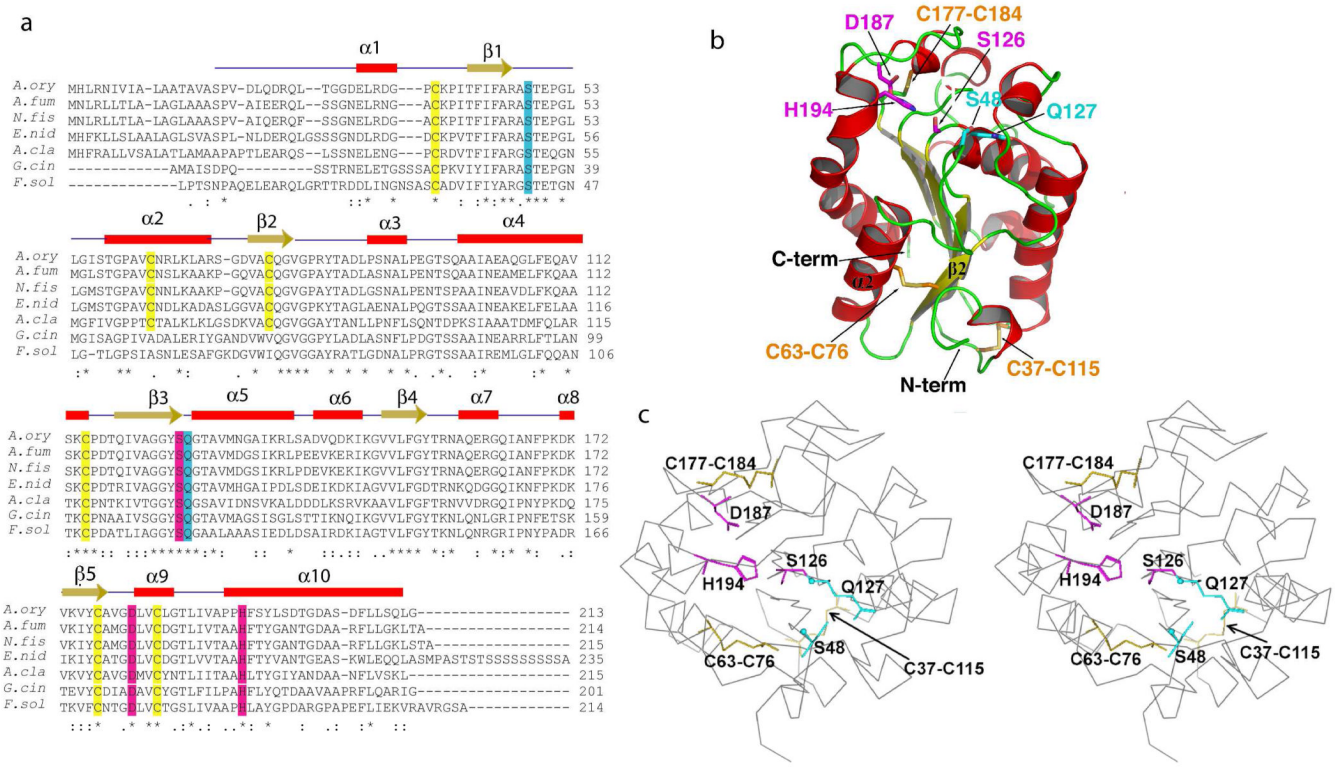

Figure 2.

(a) Sequence alignment of *Aspergillus oryzae* cutinase with cutinases originating from representative filamentous fungi with sequence identity ≥ 50%. The α-helical regions are highlighted in red, β-strands in yellow, catalytic residues in magenta, oxyanion hole residues in cyan and cysteines bearing disulfide bonds in yellow. Residues identical in all sequences in the alignment are labeled with *, Residues with conserved substations are labeled with :, and with . for semi-conserved substitutions. The alignment was performed using NCBI BLAST (http://blast.ncbi.nlm.nih.gov/) and EBI ClustalW (http://www.ebi.ac.uk/Tools/clustalw2/). (b) Ribbon structure rendering of *A. oryzae* cutinase with the helices, strands and catalytic residues labeled as in the alignment. The disulfide bonds between the cysteines are displayed in yellow. (c) Stereoview of *A. oryzae* cutinase with catalytic triad in magenta and oxyanion hole in cyan. Abbreviations: *Aspergillus oryzae- A.ory*; *Aspergillus fumigatus- A.fum*; *Aspergillus clavatus- A.cla*; *Emericella nidulans- E.nid*; *Neosartorya fischeri- N.fis; Glomerella cingulata- G.cin*; *Fusarium solani- F.sol*.

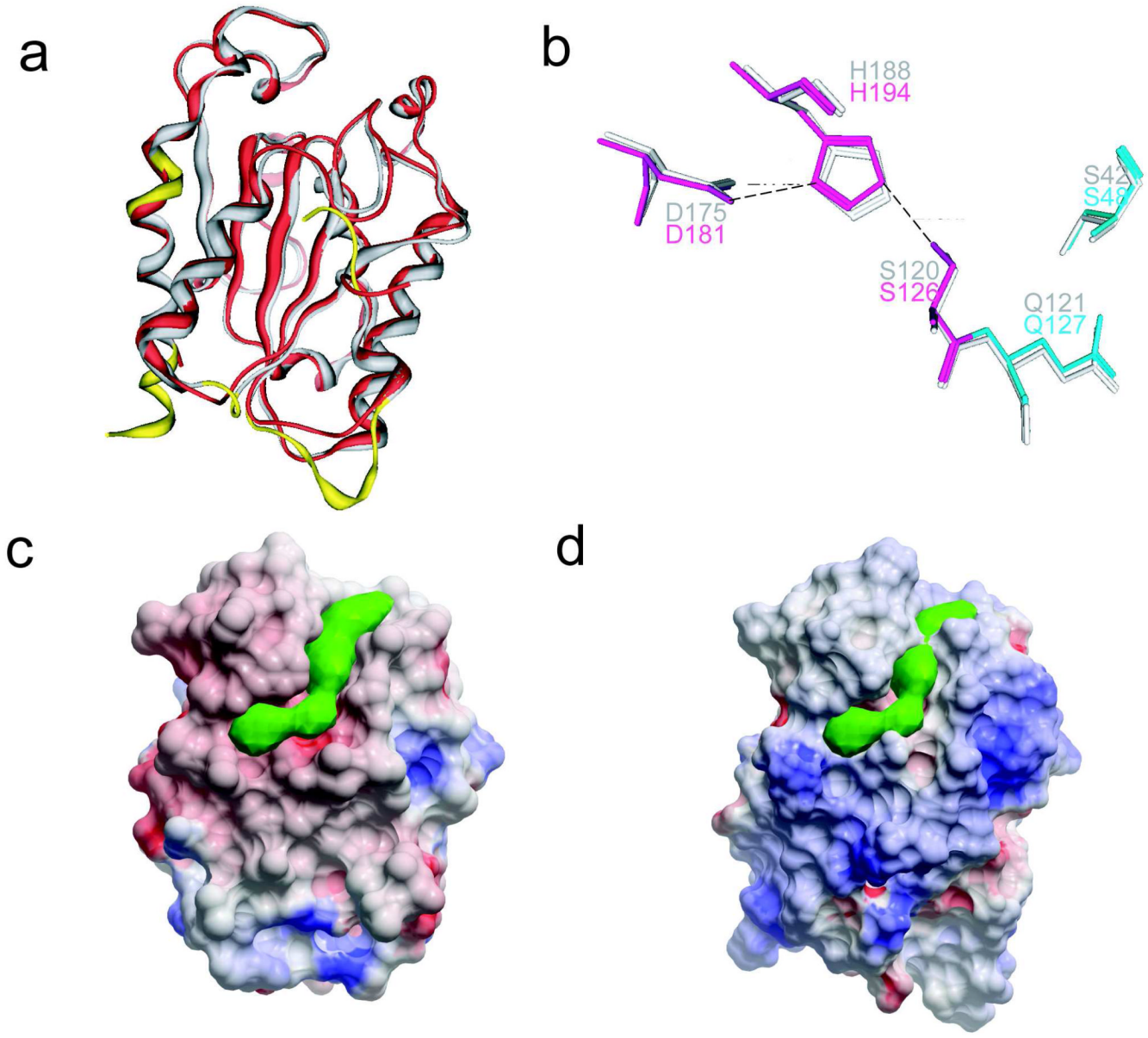

Figure 3.

(a) Superposition of A. oryzae (red) and *F. solani* (grey) cutinases revealing nearly identical structural similarity. The non-overlapping regions are highlighted in yellow. (b) Overlay of the *A. oryzae* cutinase (colored) residues of the catalytic triad and oxyanion hole with that of *F. solani* residues (grey). Residues are labeled accordingly. Electrostatic surface rendering of *A. oryzae* (c) and *F. solani* (d) cutinases as rendered by ICM software package.[28] The green solid density generated by the PocketFinder function of ICM illustrates the groove on the surface proximal to the active site.[28] Note that the green density cannot fit in the narrow groove on the *F. solani* cutinase.

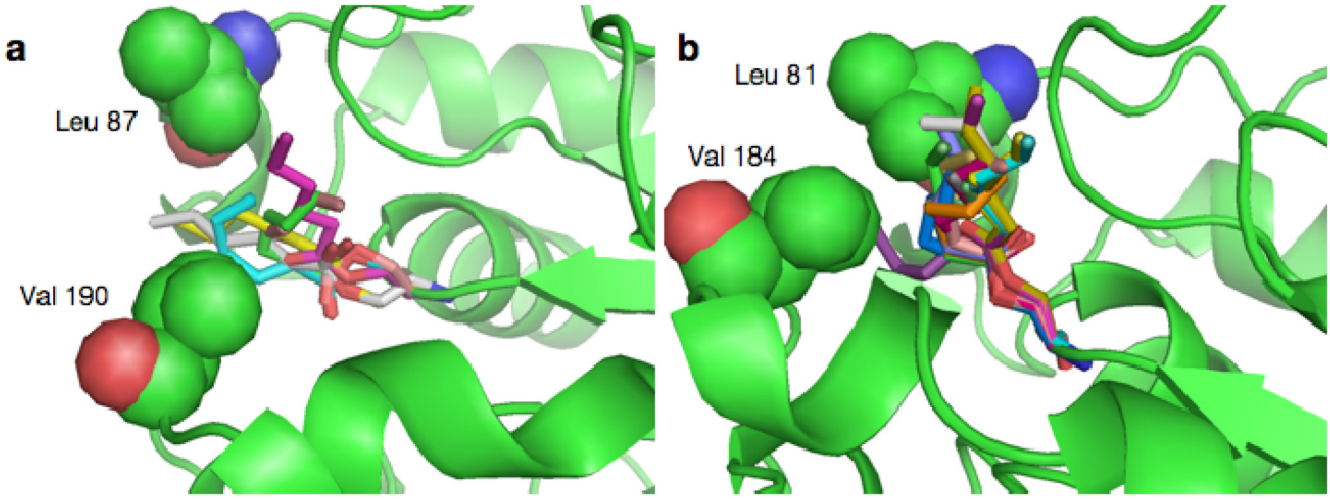

Figure 4.

Predicted low energy conformations of serine hexanoate esters for (a) *A. oryzae* and (b) *F. solani* cutinases. Ester heavy atoms are shown as sticks for all conformations within 5 kcal•mol^{-1} of the lowest energy conformation after systematic screening of torsions and minimization. The gatekeeper residues, Leu 87 and Val 190 in *A. oryzae* and Leu 81 and Val 184 in *F. solani* are shown as spheres.

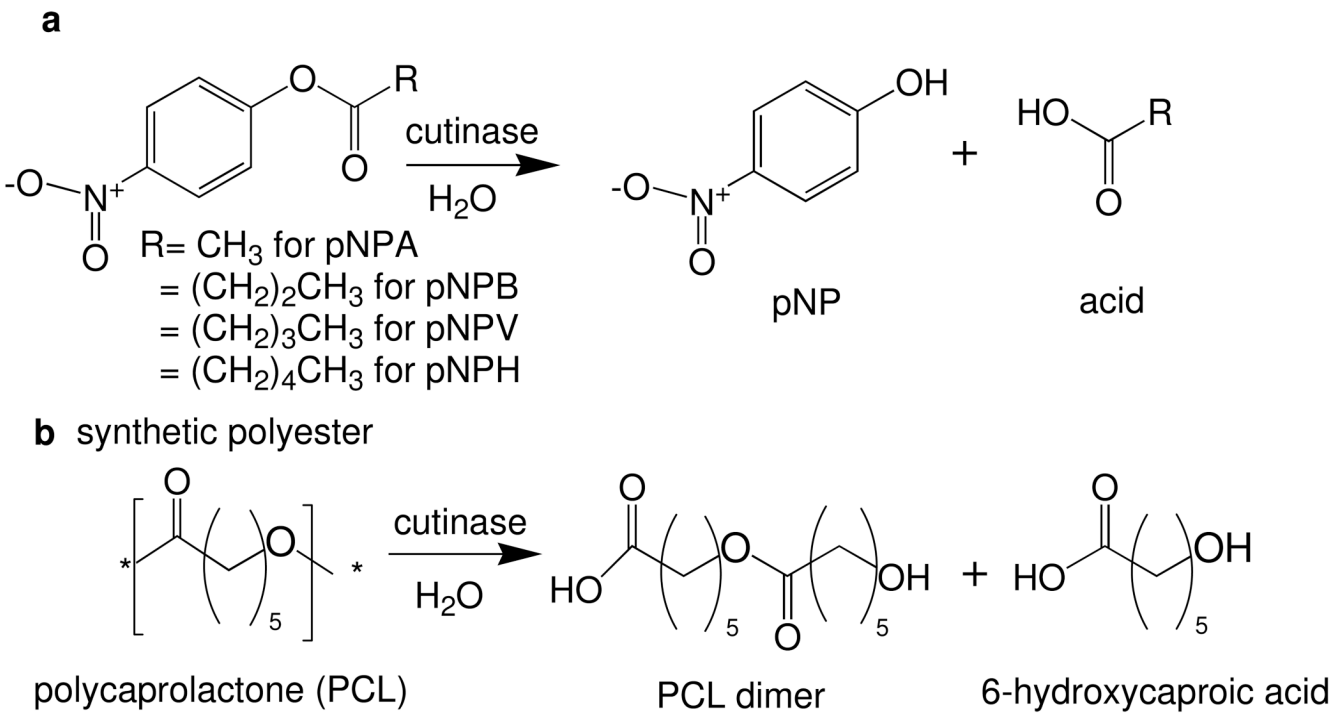

Scheme 1.

(a) Synthetic ester and (b) polyester used as substrates for hydrolytic reactions with cutinase. Abbreviations: *p*-nitrophenylacetate- pNPA; *p*-nitrophenylbutyrate- pNPB; *p*-nitrophenylvalerate-pNPV; *p*-nitrophenylhexanoate- pNPH; polycaprolactone- PCL.

Table 1

Kinetic and Thermodynamic Parameters

Cutinase	pNPA		pNPB		pNPV		pNPH		T_m (°C)	ΔH (kJ/mol)
	K_m (μM^{-1})	k_{cat}/K_m ($\mu M^{-1}min^{-1}$)	K_m (μM^{-1})	k_{cat}/K_m ($\mu M^{-1}min^{-1}$)	K_m (μM^{-1})	k_{cat}/K_m ($\mu M^{-1}min^{-1}$)	K_m (μM^{-1})	k_{cat}/K_m ($\mu M^{-1}min^{-1}$)		
F. solani	0.67 ± 0.23	2.53 ± 1.11	1.26 ± 0.28	0.26 ± 0.06	1.48 ± 0.56	0.61 ± 0.40	1.50 ± 0.19	0.14 ± 0.02	56	562.21
A. oryzae	4.96 ± 0.11	0.07 ± 0.01	0.21 ± 0.04	3.49 ± 0.51	0.04 ± 0.01	3.32 ± 0.74	0.29 ± 0.09	1.34 ± 0.48	59	622.61